Fractional Regularized Distorted Born Iterative Method for Permittivity Reconstruction

Amit MAGDUM [1], Mallikarjun ERRAMSHETTY [1], Ravi Prasad K. JAGANNATH [2]

[1] Dept. of Electronics and Communication Engineering, National Institute of Technology Goa, India
[2] Dept. of Applied Sciences, National Institute of Technology Goa, India

{amitmagdum, emallikarjuna, k.j.raviprasad}@nitgoa.ac.in

Abstract.   *In this paper, we propose a fractional regularized distorted Born iterative method (DBIM) to solve non-linear ill-posed problems of microwave imaging. Fractional regularization is a modification to Tikhonov regularization, where singular values are weighed with fractional power. As a result, the well-known effect of oversmoothing present in Tikhonov regularization is reduced, thereby the output image quality is improved. The results of this method are compared with standard DBIM using Tikhonov regularization. Various numerical examples of simulated and experimental datasets containing homogeneous as well as heterogeneous scatterers are considered to validate the effectiveness of the proposed approach. It is found that the proposed method improves the accuracy of estimated images over conventional DBIM.*

Keywords

Distorted Born iterative method, fractional regularization, ill-posed problem, microwave imaging, Tikhonov regularization

1.   Introduction

Microwave imaging (MWI) is an electromagnetic sensing technique for detecting the properties of unknown objects from multi-view, multi-static measured scattered field data [1], [2]. MWI methods are classified as qualitative and quantitative methods. Qualitative methods provide only the morphological features (size, shape, and position) of the target. However, quantitative methods provide additional electrical features (permittivity, conductivity, etc.) associated with the target. Quantitative reconstruction problems are non-linear and ill-posed in nature. These problems can be solved easily with the help of non-iterative methods, which assume certain conditions to simplify the problem [3]. However, this assumption does not consider the effect of multiple scattering associated with strong dielectric objects. This effect causes distortion in the reconstruction and results in ghost images [4]. In order to overcome this difficulty, an iterative approach needs to be developed where the relation between scattered field and permittivity profile is non-linear.

Generally, in this approach, the objective function for optimization is constructed by the measure of the mismatch between the collected scattered field and the calculated scattered field. The unknown permittivity is obtained by minimizing this objective function. In the literature, many optimization schemes have been proposed to evaluate this objective function. Among them, the Born iterative method (BIM) [5], contrast source inversion (CSI) [6], distorted Born iterative method (DBIM) [4], [7], and subspace optimization method (SOM) [8] are the most widely used techniques. The DBIM is an extensively used regularized iterative algorithm because of its simplicity and fast convergence rate. This method requires a regularization procedure to obtain a convergent solution. Several regularization techniques have been proposed in literature, most notably, Truncated Singular Value Decomposition (TSVD) [9], and Tikhonov regularization (TR) [10], [11]. The basic idea behind TSVD is to reduce the condition number by neglecting the least significant singular values [1], [9]. However, the choice of condition number depends on the noise level in the data. Also, the choice of the smallest considered singular value is often a critical issue. The TR method is recognized as the widely considered filtering technique aimed at minimizing the residual with the penalty term [12], [13]. However, it suffers from the well-known effect of oversmoothing [14]. In this case, fine or sharp features of the image are lost, which can be troublesome in critical applications, where it is of high priority to recover. This effect can be reduced by modifying the related filter factors by introducing the fractional power term, and this technique is called fractional regularization (FR) [14–16]. This modification allows controlling the amount of smoothness or damping in the reconstructed solution and leads to a more accurate reconstruction. In this work, the FR based DBIM is applied to the numerical examples of synthetic and experimental data [17], [18], and the results are found encouraging.

This paper is structured as follows. Section 2 formulates the inverse scattering problem, which explains the mathematical basis of inversion methods. Section 3 provides a detailed description of a proposed algorithm. Numerical simulations and results are presented in Sec. 4. The discussion and brief conclusion of the work is drawn at the end in Sec. 5.

2. Problem Formulation

For simplicity, we consider the two-dimensional inverse scattering problem of transverse magnetic polarization. To determine the relationship between the contrast function and the scattered field, the scattering equations are represented as,

$$E^{\mathrm{t}}(\underline{r}) = E^{\mathrm{i}}(\underline{r}) + \mathrm{j}\omega\mu_{\mathrm{b}} \int \chi(\underline{r}')E^{\mathrm{t}}(\underline{r}')G(\underline{r},\underline{r}')\mathrm{d}\underline{r}', \ \underline{r},\underline{r}' \in \Delta, \tag{1}$$

$$E^{\mathrm{s}}(\underline{r}) = \mathrm{j}\omega\mu_{\mathrm{b}} \int \chi(\underline{r}')E^{\mathrm{t}}(\underline{r}')G(\underline{r},\underline{r}')\mathrm{d}\underline{r}', \quad \underline{r} \in \Omega, \underline{r}' \in \Delta \tag{2}$$

where E^{t}, E^{i} and E^{s} are the total field, the incident field, and the scattered field, respectively. The spatial variables $\underline{r}, \underline{r}' \in$ (x,y) denotes the Cartesian coordinates of the measurement point and the source point, respectively, $G(\underline{r},\underline{r}')$ is the free space Green's function, and χ is the contrast function, which is defined as $\chi(r) = [\epsilon_{\mathrm{r}}(r)/\epsilon_{\mathrm{b}} - 1]$, where ϵ_{b} and ϵ_{r} is the relative permittivity of the background and the object, respectively. The test domain and observation domain are represented by Δ and Ω, respectively. From the use of method of moments [19], Equation (1) and (2) can be discretized. Consequently, the discretized expressions in the matrix form are [20]

$$\mathbf{E}^{\mathrm{t}} = \mathbf{E}^{\mathrm{i}} + \left[G^{\Delta}\right]\left[E^{\mathrm{t}}\right]\boldsymbol{\chi}, \tag{3}$$

$$\mathbf{E}^{\mathrm{s}} = \left[G^{\Omega}\right]\left[E^{\mathrm{t}}\right]\boldsymbol{\chi} \tag{4}$$

where $\left[G^{\Delta}\right]$ and $\left[G^{\Omega}\right]$ are the internal and external radiation operators, respectively. Here, the variables in bold letter indicate the vector, and the variables in $[\cdot]$ indicate the matrix. In the inverse scattering problem, $\mathbf{E}^{\mathrm{i}}$, $\left[G^{\Delta}\right]$, $\left[G^{\Omega}\right]$, and $\mathbf{E}^{\mathrm{s}}$ are known quantities, whereas $\boldsymbol{\chi}$ and $\left[E^{\mathrm{t}}\right]$ are unknown terms. The problem of finding $\boldsymbol{\chi}$ from these equations is non-linear.

3. Fractional Regularized Distorted Born Iterative Method

The DBIM is a popular quantitative approach that estimates solutions to the non-linear inverse scattering problems by successive linear approximations [4]. In this approach, at each iteration, the Green's function is also updated [3]. Here, the optimization problem consists of determining the deviation in scattering contrast $\delta\chi$ inserted inside an inhomogeneous background. A penalty term is introduced to stabilize the optimization. The objective function is selected as the L^2-norm of mismatch of the collected and calculated scattered field as

$$f(\delta\chi) = \sum_{p=1}^{N} \left\|\mathbf{E}_P^{\mathrm{s}} - \left[G^{\Omega}\right][\chi]\mathbf{E}_P^{\mathrm{b}} - \left[G^{\mathrm{b}}\right][\delta\chi]\mathbf{E}_P^{\mathrm{b}}\right\|^2$$
$$+ \lambda\|\boldsymbol{\delta\chi}\|^2 \tag{5}$$

where N ($p = 1, 2, \cdots, N$) is the number of incident fields, $\mathbf{E}_P^{\mathrm{b}}$ is the secondary incident field in the presence of inhomogeneous background medium, $\left[G^{\mathrm{b}}\right]$ is an inhomogeneous background Green's function operator, and λ is the regularization parameter. The principle steps for solving the nonlinear integral equation using the regularized iterative DBIM are briefly described below.

1. Initialize with $n = 0$, $\mathbf{E}_P^{\mathrm{b}} = \mathbf{E}_P^{\mathrm{i}}$, $\boldsymbol{\delta\chi}_n = 0$.

2. Find the secondary incident field as

$$\mathbf{E}_{p,n}^{\mathrm{b}} = \left(\left[I\right] - \left[G^{\Delta}\right]\left[\chi_n\right]\right)^{-1}\mathbf{E}_p^{\mathrm{i}}. \tag{6}$$

3. Update the Green's function as

$$\left[G_n^{\mathrm{b}}\right] = \left[G^{\Omega}\right]\left(\left[I\right] - \left[\chi_n\right]\left[G^{\Delta}\right]\right)^{-1}. \tag{7}$$

4. Calculate the kernel matrix $[G]$ and the data vector $\mathbf{h}$ as

$$\left[G_{p,n}\right] = \left[G_n^{\mathrm{b}}\right]\left[E_{p,n}^{\mathrm{bac}}\right], \tag{8}$$

$$\mathbf{h}_{p,n} = \mathbf{E}_p^{\mathrm{s}} - \left[G^{\Omega}\right]\left[\chi_n\right]\mathbf{E}_{p,n}^{\mathrm{b}}. \tag{9}$$

5. Estimate $\boldsymbol{\delta\chi}_n$ by solving the linear equation

$$\left[G_{p,n}\right]\boldsymbol{\delta\chi}_n = \mathbf{h}_{p,n}. \tag{10}$$

6. Update the contrast function as $\boldsymbol{\chi}_{n+1} = \boldsymbol{\chi}_n + \boldsymbol{\delta\chi}_n$.

7. Return to step 2 and proceed until solution converges.

The convergence of the solution depends highly on the ill-posed problem of (10) as it updates regularized solution for each iteration. In order to solve such problem, this paper is concerned with the estimation of an approximate solution to the linear least-squares problem

$$\min_{\boldsymbol{\delta\chi}}\|[G]\boldsymbol{\delta\chi} - \mathbf{h}\|. \tag{11}$$

Specifically, $[G]$ is a severely ill-conditioned matrix, and such problems are often called discrete ill-posed problems. Vector $\mathbf{h}$ denotes the available data, which is corrupted by the error $\boldsymbol{\xi}$. Errors may arise from measurement inaccuracies or discretization. Therefore, $\mathbf{h} = \hat{\mathbf{h}} + \boldsymbol{\xi}$, where $\hat{\mathbf{h}}$ represents the unknown errorless vector associated with $\mathbf{h}$. The solution of the least-squares problem (11) is usually a poor estimate of the exact solution, due to the ill-conditioning of the matrix $[G]$ and the error $\boldsymbol{\xi}$ in $\mathbf{h}$. Therefore, it requires a regularization strategy to obtain an approximate solution. In general, the TR is used to solve this problem [4], [21]. However, it suffers from the effect of oversmoothing. Therefore, in this work, an FR approach is implemented to determine the approximation of a solution. This scheme replaces the minimization problem with the penalized least squares problem, where the data fidelity term is penalized using the weight matrix [14] [15]. Therefore, the penalized least squares objective function can be given as

$$\Psi = \min_{\boldsymbol{\delta\chi}}(\|[G]\boldsymbol{\delta\chi} - \mathbf{h}\|_W^2 + \lambda\|\boldsymbol{\delta\chi}\|_2^2) \tag{12}$$

where $\|\boldsymbol{\delta\chi}\|_W = \left(\boldsymbol{\delta\chi}^* [W] \, \boldsymbol{\delta\chi}\right)^{1/2}$ and $[W]$ is the symmetric positive semidefinite matrix defined as $[W] = \left([G] \, [G]^*\right)^{\frac{\gamma-1}{2}}$, where $\gamma > 0$ represents fractional power, which controls the degree of smoothness or damping by increasing the norm of the estimated solution [15]. Seminorm $\|.\|_W$ allows the γ to be selected in such a way that the solution obtained in (12) is of good quality. By differentiating (12) with respect to $\boldsymbol{\delta\chi}$ and equating to zero leads to

$$\left(\left([G]^* [G]\right)^{\frac{\gamma+1}{2}} + \lambda I\right) \boldsymbol{\delta\chi} = \left([G]^* [G]\right)^{\frac{\gamma-1}{2}} [G]^* \, \mathbf{h}. \quad (13)$$

The singular value decomposition (SVD) is a powerful tool to solve linear inverse problems. By using SVD, the system matrix $[G]$ can be represented as

$$[G] = [U] \, [\Sigma] \, [V]^* \quad (14)$$

where $[U] = [\mathbf{u}_1, \mathbf{u}_2, \ldots, \mathbf{u}_M]$ and $[V] = [\mathbf{v}_1, \mathbf{v}_2, \ldots, \mathbf{v}_N]$ are orthogonal matrices and are called as the left and right singular matrices of $[G]$, respectively, and $[\Sigma] = \text{diag} \, [\sigma_1, \sigma_2, \ldots, \sigma_N]$ is the diagonal singular value matrix. Here $*$ represents the conjugate transpose operator. By substituting the SVD (14) into (13) yields

$$\left([V] \, [\Sigma] \, [U]^* \, [U] \, [\Sigma]^{\gamma-1} \, [U]^* \, [U] \, [\Sigma] \, [V]^* + \lambda I\right) \boldsymbol{\delta\chi} =$$
$$[V] \, [\Sigma] \, [U]^* \, [U] \, [\Sigma]^{\gamma-1} \, [U]^* \, \mathbf{h}, \quad (15)$$

$$\left([V] \, [\Sigma]^{\gamma+1} \, [V]^* + \lambda I\right) \boldsymbol{\delta\chi} = [V] \, [\Sigma]^{\gamma} \, [U]^* \, \mathbf{h}. \quad (16)$$

The solution to this equation is given by

$$\boldsymbol{\delta\chi} = \sum_{i=1}^{r} \frac{\sigma_i^{\gamma}}{\sigma_i^{\gamma+1} + \lambda} \langle \mathbf{h}, \mathbf{u}_i \rangle \, \mathbf{v}_i \quad (17)$$

where $r \leq N$ denotes the rank of the system matrix. It is important to note that FR scales the singular values based on the amount of fractional power. The choice of λ depends on the amount of error $\boldsymbol{\xi}$ in $\mathbf{h}$. In general, the larger $\|\boldsymbol{\xi}\|$, the larger λ should be. However, it follows from (17) that increasing λ reduces the norm of the calculated solution. Therefore, the calculated solution may have a substantially smaller norm than the expected solution. This difficulty can be overcome by selecting $\gamma < 1$ because it increases the norm of the calculated solution. The filter factor for the fractional regularization is given by

$$\phi^{\text{frac}}(\sigma) = \frac{\sigma^{\gamma}}{\sigma^{\gamma+1} + \lambda}. \quad (18)$$

The filtering factors are intended to suppress the contribution of insignificant singular terms to the solution, thereby providing a more stable and non-oscillating solution. The asymptotics of the filter function are

$$\phi^{\text{frac}}(\sigma) = \frac{\sigma^{\gamma}}{\lambda} + O\left(\sigma^{2\gamma+1}\right) \quad (\sigma \to 0), \quad (19)$$

$$\phi^{\text{frac}}(\sigma) = \frac{1}{\sigma} + O\left(\sigma^{-(\gamma+2)}\right) \quad (\sigma \to \infty). \quad (20)$$
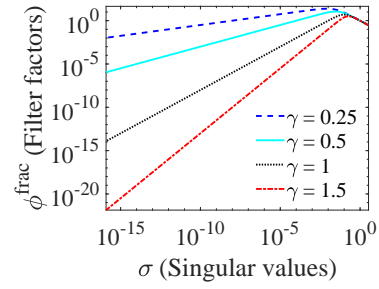

Fig. 1. Comparison of filter factors with respect to σ, for different values of γ.

Figure 1 displays the plot of ϕ^{frac} for $\lambda = 0.01$ and different values of γ. It can be seen that the contribution of minor components is damped. Filter factors differ in how fast they converge to 0 when σ reduces to 0. Fast convergence indicates significant smoothing of the estimated solution. Here, $\gamma = 1$ indicates the Tikhonov filter factor $\left(\phi^{\text{tikh}}\right)$. The asymptotic behaviour of $\phi^{\text{frac}}(\sigma)$ as $\sigma \to 0$ shows this function provides less smoothing than the $\phi^{\text{tikh}}(\sigma)$ for $0 < \gamma < 1$. The components of the solution corresponding to small singular values are damped less by the $\phi^{\text{frac}}(\sigma)$ function. This often produces the solution of higher quality than TR.

4. Reconstruction Results

In this section, numerical simulations are performed to examine the performance of the fractional regularization for dielectric objects (homogeneous as well as heterogeneous scatterers). For the purpose of reconstruction, the size of Δ is considered to be $20\,\text{cm} \times 20\,\text{cm}$ and subdivided into 1681 cells (41×41). The permittivity of the background medium is considered as $\epsilon_\text{b} = 1$. The reconstruction is carried out at a working frequency of $3\,\text{GHz}$ and adopted with synthetic as well as experimental data (made available by the Institute of Fresnel, France [17], [18]). In all cases, a $\gamma = 0.6$ value is used for reconstruction, which is selected empirically based on observations.

In order to quantify the reconstruction performance of the algorithms, two important parameters are introduced. These are the mean square error (MSE) and the Pearson's correlation coefficient (PCC). The MSE can be computed as

$$MSE = \frac{\|\epsilon_\text{r} - \hat{\epsilon}_\text{r}\|^2}{\|\epsilon_\text{r}\|^2} \quad (21)$$

where ϵ_r and $\hat{\epsilon}_\text{r}$ denotes the original and the estimated permittivity, respectively. Similarly, the PCC can be defined as [15]

$$PCC\left(\epsilon_\text{r}, \hat{\epsilon}_\text{r}\right) = \frac{\text{cov}\left(\epsilon_\text{r}, \hat{\epsilon}_\text{r}\right)}{s\left(\epsilon_\text{r}\right) s\left(\hat{\epsilon}_\text{r}\right)} \quad (22)$$

where cov denotes the covariance and s denotes the standard deviation. This coefficient varies in the range of -1 to 1. Larger value of PCC is desirable as it indicates detectability of the target.

4.1 Tests on Synthetic Data

In the synthetic examples, the scatterer under test is illuminated by a plane wave at angles of $0°$, $15°$, $\cdots$, $345°$ and the resulted scattered fields in the far-field are measured along the same angles. Here, the value of ϵ_r is chosen such that $\left\| \left[G^\Delta \right] \chi \right\| > 1$ for the considered frequencies so that the object can be treated as a strong scatterer [22]. Three examples are used in this section to demonstrate the efficiency of the proposed method.

4.1.1 L-shape Structure with Multilayer Cylinder

In this example, a complicated synthetic data profile is inspected. As shown in Fig. 2, this example consists of one L-shaped dielectric cylinder with $\epsilon_r = 1.75$, and a multilayer object with permittivity of inner and outer cylinders equal to 2 and 1.5, respectively. The two-layer circular concentric cylinder is centered at $(4, 0)$ cm, with inner and outer radii of 1.5 and 5 cm, respectively. This configuration is inhomogeneous that includes both weak and strong scattering parts. A stratified elliptic cylinder is sufficiently complex to provide a good test for numerical algorithms [1]. Figures 2(b)–(f) show the reconstructed distributions of the permittivity. It can be seen that the results with the fractional method are

close to the reference profile. The behavior of MSE with respect to iteration number is reported in Fig. 2(d). The result shows that the error is minimum for the proposed method. Furthermore, the PCC values are plotted in Fig. 2(e). It shows that the FR has a high value of PCC compared to TR. In addition, as illustrated in Fig. 2(f), the permittivity value is plotted in a one-dimensional (1D) plot. It displays the permittivity values of the original and reconstructed profiles along the x-axis ($y = 0$). As can be observed in this graph, the proposed technique reconstructs the target accurately.

4.1.2 Austria Profile

The algorithm is then validated on the Austria profile, which is a challenging and well-known configuration in the inverse scattering community [3] [23]. It consists of a ring with inner and outer radii of 3 cm and 6 cm, respectively, and two discs with radii of 2 cm each. The ring is centered at $(0, -2)$ cm, while the discs are centered at $(3, 6)$ cm and $(-3, 6)$ cm, respectively. The permittivity distribution of this target is uniform, with $\epsilon_r = 2$. Figure 3 depicts the reconstruction results, which show that the proposed algorithm produces more precise reconstruction. The evaluation metrics (MSE, PCC and 1D plot) values show that the proposed technique is more accurate than the TR-based DBIM.
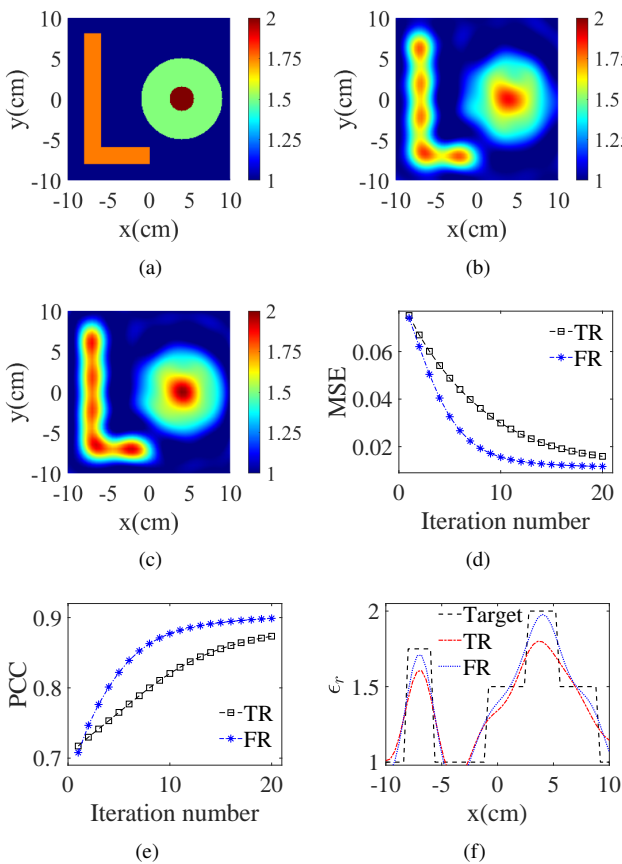

Fig. 2. Synthetic data results for L-shape structure with multilayer cylinder: (a) Original profile, (b) DBIM using TR, (c) DBIM using FR, (d) MSE, (e) PCC, (f) 1D plot along x-axis ($y = 0$).
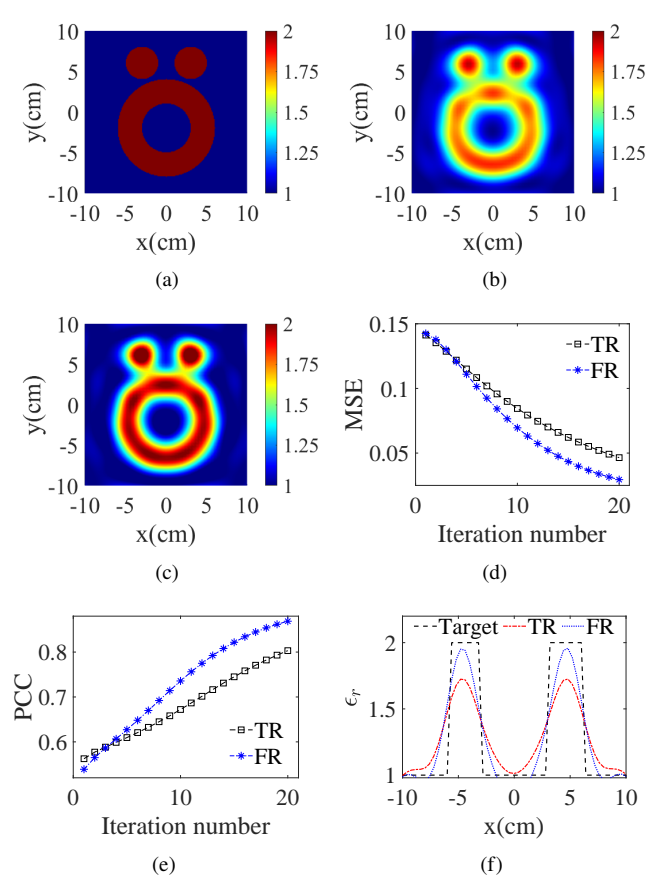

Fig. 3. Synthetic data results for Austria profile: (a) Original profile, (b) DBIM using TR, (c) DBIM using FR, (d) MSE, (e) PCC, (f) 1D plot along the center of the ring.

4.1.3 U-shaped Profile

In this example, we have considered the non-convex target, such as the U-shaped scatterer. The effect of multiple scattering is stronger here, which increases the non-linearity of the problem. The dimension of this target configuration is $(12 \times 12)\,\text{cm}^2$, as indicated in Fig. 4(a). The permittivity of this purely dielectric structure is $\epsilon_\text{r} = 2$. Figure 4 depicts the corresponding simulation results. Here again, a superior reconstruction is achieved using the proposed technique. The results of the evaluation measures show that even for non-convex scatterers, the proposed methodology is quite accurate.

4.2 Tests on Experimental Data

In this section, we will illustrate the experimental test results. We considered the datasets provided by the Institute of Fresnel, Marseille, France, which are widely used as a benchmark for inverse problems at microwave frequencies [17], [18]. It is concerned with complicated structures consisting of many materials. The test setup consists of an anechoic compartment, which consists of a transmitter, which is installed at a fixed position on the circular track, while the receiver revolves around the vertical cylindrical target. The measurement setup consists of linearly polarized double ridged horn antennas, with a wideband frequency range from 1 GHz to 18 GHz.

In experimental examples, we have considered three different target configurations. All the targets are very large along a vertical direction to form a nearly 2D structure. The first example is taken from the Fresnel dataset 2001 [17], which consists of a strongly scattering circular dielectric cylinder. Thereafter, the algorithm is tested on two inhomogeneous scatterers from the Fresnel dataset 2005 [18], *FoamDielExtTM* and *FoamTwinDielTM*.

4.2.1 Example I: Single Dielectric

For this example, the transmitting and receiving antenna were kept at a distance of 0.72 m and 0.76 m, respectively, from the center of the test region [17]. The scatterer is illuminated at an angle of $0°, 10°, \cdots, 350°$, and the scattered fields are collected at an angle of $60°, 65°, \cdots, 300°$ with respect to the corresponding emitter. The scatterer profile consists of single circular, homogeneous, dielectric cylinder of permittivity 3±0.3. The cylinder has a radius of 1.5 cm and kept at a distance of 3 cm from the origin. The reconstructed permittivity distributions at a frequency of 3 GHz are shown in Fig. 5. It can be observed that the quality of the reconstruction obtained using FR is quite good in terms of accuracy. Also, the rate of convergence is faster for this method.
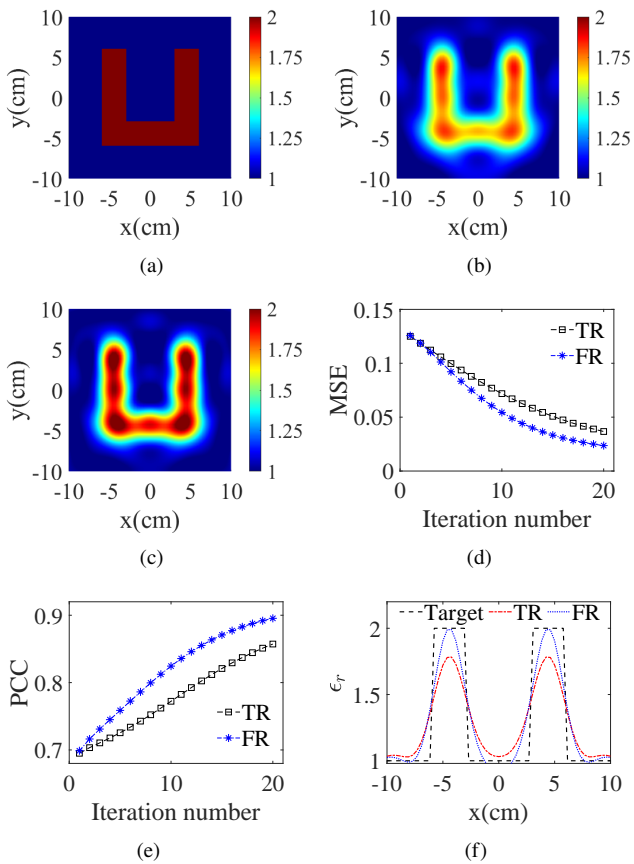

Fig. 4. Synthetic data results for U-shaped profile: (a) Original profile, (b) DBIM using TR, (c) DBIM using FR, (d) MSE, (e) PCC, (f) 1D plot along x-axis ($y = 0$)
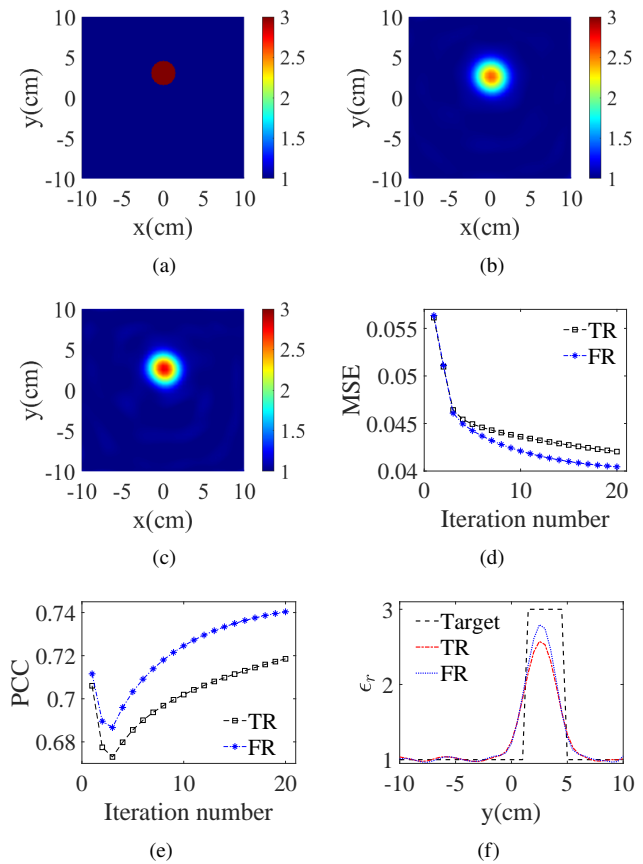

Fig. 5. Experimental data results for single dielectric cylinder: (a) Original profile, (b) DBIM using TR, (c) DBIM using FR, (d) MSE, (e) PCC, (f) 1D plot along y-axis ($x = 0$).
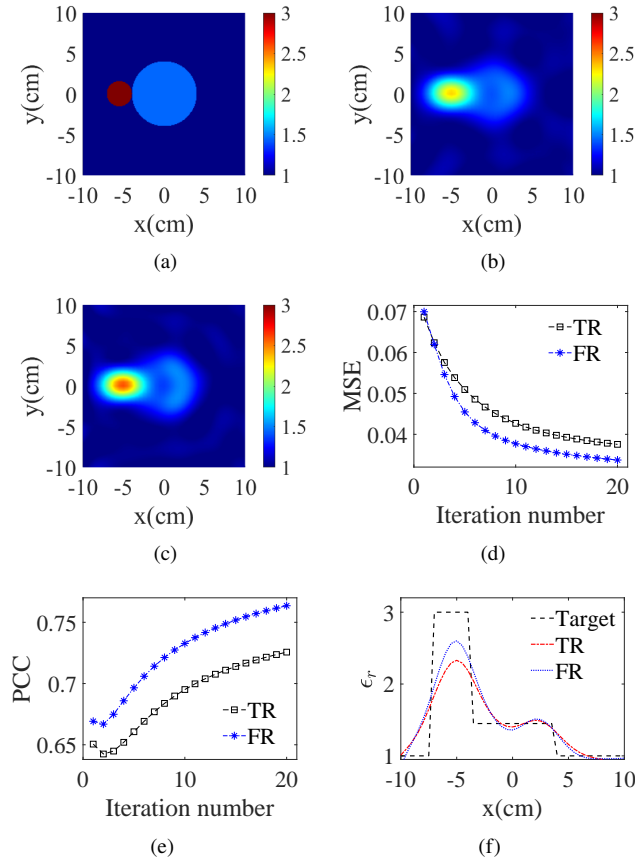
Fig. 6. Experimental data results for *FoamDielExtTM*: (a) Original profile, (b) DBIM using TR, (c) DBIM using FR, (d) MSE, (e) PCC (f), 1D plot along x-axis ($y = 0$).
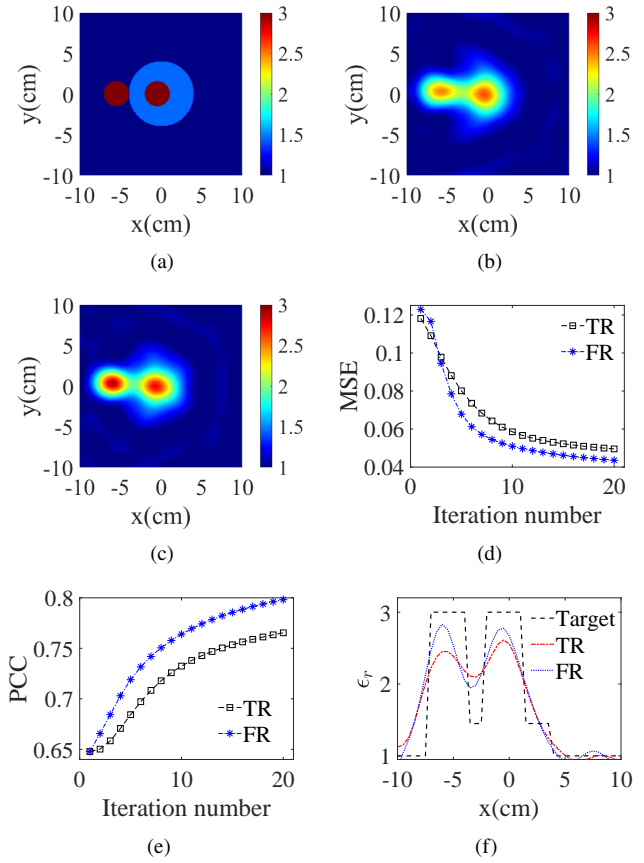

Fig. 7. Experimental data results for *FoamTwinDielTM*: (a) Original profile, (b) DBIM using TR, (c) DBIM using FR, (d) MSE, (e) PCC, (f) 1D plot along x-axis ($y = 0$).

4.2.2 Example II: FoamDielExtTM

In this example, the scatterer is illuminated at an angle of $0°$, $45°$, $\cdots$, $315°$, and the scattered fields are collected at an angle of $60°$, $61°$, $\cdots$, $300°$ with respect to the corresponding emitter. The transmitting and receiving antenna were kept at a distance of 1.67 m from the center of the test region [18]. As shown in Fig. 6(a), the scatterer profile consists of two circular dielectric cylinders. The first one consists of a centered foam cylinder with a radius of 4 cm and permittivity of 1.45 ± 0.15. Another target consists of a plastic cylinder of radius 1.55 cm, permittivity 3 ± 0.3, placed at a distance of 5.55 cm from the origin. The reconstructed permittivity distributions after 20 iterations are displayed in Fig. 6. Here again, excellent reconstructions are obtained (visibly and quantitatively) with the proposed method.

4.2.3 Example III: FoamTwinDielTM

Finally, in this example, a more complex target is inspected. As shown in Fig. 7(a), this target configuration is the same as used in Example II, except that there is an additional plastic cylinder inside the foam cylinder. This geometry of

the target is favorable to the occurrence of multiple scattering. The simulation results at a frequency of 3 GHz are shown in Fig. 7(b)–(f). From the results, it is observed that the profile of the target is clearly and most accurately identified by the fractional regularization approach.

5. Conclusion

A fractional regularization based distorted Born iterative method (DBIM) is studied for the reconstruction of two-dimensional dielectric scatterers of Microwave imaging. It introduces the fractional power term (γ) for weighing singular values, which can control the smoothness of the solution. Applying this scaling to singular values results in a better reconstruction. The performance of this algorithm is evaluated using numerical examples of simulated and experimental data. In all the cases, the proposed method has a faster convergence rate and produces higher reconstruction quality compared to the conventional Tikhonov regularization based DBIM. Furthermore, it has been shown that the error in the output is minimum for this method.

References

[1] PASTORINO, M. *Microwave Imaging*. Hoboken (USA): John Wiley & Sons, 2010. ISBN: 9780470278000

[2] NIKOLOVA, N. *Introduction to Microwave Imaging*. Cambridge (UK): Cambridge University Press, 2017. ISBN: 9781316084267

[3] CHEN, X. *Computational Methods for Electromagnetic Inverse Scattering*. Singapore: John Wiley & Sons, 2018. ISBN: 9781119311980

[4] CHEW, W., WANG Y. Reconstruction of two-dimensional permittivity distribution using the distorted Born iterative method. *IEEE Transactions on Medical Imaging*, 1990, vol. 9, p. 218–225. DOI: 10.1109/42.56334

[5] JUN, S., CHOI, U. Convergence analyses of the born iterative method and the distorted born iterative method. *Numerical Functional Analysis and Optimization*, 1999, vol. 20, no. 3-4, p. 301–316. DOI: 10.1080/01630569908816893

[6] BERG, P., KLEINMAN R. A contrast source inversion method. *Inverse Problems*, 1997, vol. 13, no. 6, p. 1607–1620. DOI: 10.1088/0266-5611/13/6/013

[7] LIU, H., YE, X. Reconstruction of dielectric parameters of human tissues using distorted Born iterative method. In *IEEE International Conference on Computational Electromagnetics (ICCEM)*. Shanghai (China), 2019, p. 1–2. DOI: 10.1109/COMPEM.2019.8778947

[8] YE, X., CHEN, X. Subspace-based distorted-Born iterative method for solving inverse scattering problems. *IEEE Transactions on Antennas and Propagation*, 2017, vol. 65, no. 12, p. 7224–7232. DOI: 10.1109/TAP.2017.2766658

[9] FANJUN, L., XIAOHONG, W., YING, L., et al. Regularized ESN based on TSVD. In *Chinese Automation Congress (CAC)*. Xi'an (China), 2018, p. 3312–3316. DOI: 10.1109/CAC.2018.8623332

[10] MUELLER, J., SILTANEN S. *Linear and Nonlinear Inverse Problems with Practical Applications*. Philadelphia (USA): Society for Industrial and Applied Mathematics, 2020. ISBN: 9781611972337

[11] MAGDUM, A., ERRAMSHETTY, M., JAGANNATH, R. Regularized minimal residual method for permittivity reconstruction in microwave imaging. *Microwave and Optical Technology Letters*, 2020, vol. 62, no. 8, p. 1–13. DOI: 10.1002/mop.32487

[12] ZHDANOV, M. *Geophysical Inverse Theory and Regularization Problems*. Amsterdam (Netherlands): Elsevier Science, 2002. ISBN: 0444510893

[13] ASTER, R., THURBER, C., BORCHERS, B. *Parameter Estimation and Inverse Problems*. Boston (USA): Elsevier Academic Press, 2005. DOI: 10.1016/C2009-0-61134-X

[14] HOCHSTENBACH, M., REICHEL, L. Fractional Tikhonov regularization for linear discrete ill-posed problems. *BIT Numerical Mathematics*, 2011, vol. 51, no. 1, p. 197–215. DOI: 10.1007/s10543-011-0313-9

[15] PRAKASH, J., SANNY, D., KALVA, S., et al. Fractional regularization to improve photoacoustic tomographic image reconstruction. *IEEE Transactions on Medical Imaging*, 2019, vol. 38, p. 1935–1947. DOI: 10.1109/TMI.2018.2889314

[16] KLANN, E., RAMLAU, R. Regularization by fractional filter methods and data smoothing. *Inverse Problems*, 2008, vol. 24, no. 2. DOI: 10.1088/0266-5611/24/2/025018

[17] BELKEBIR, K., SAILLARD, M. Special section: Testing inversion algorithms against experimental data. *Inverse Problems*, 2001, vol. 17, no. 6, p. 1565–1571. DOI: 10.1088/0266-5611/17/6/301

[18] GEFFRIN, J., SABOUROUX, P., EYRAUD, C. Free space experimental scattering database continuation: Experimental set-up and measurement precision. *Inverse Problems*, 2005, vol. 21, no. 6. DOI: 10.1088/0266-5611/21/6/S09

[19] PETERSON, A., RAY, S., MITRA, R. *Computational Methods for Electromagnetics*. Wiley-IEEE Press, 1998. ISBN: 9780780311220

[20] MAGDUM, A., ERRAMSHETTY, M., JAGANNATH, R. An exponential filtering based inversion method for microwave imaging. *Radioengineering*, 2021, vol. 30, no. 3, p. 496–503. DOI: 10.13164/re.2021.0496

[21] ALTUNCU, Y., DURUKAN, T., AKDOGAN, R. Reconstruction of two-dimensional objects buried into three-part space with locally rough interfaces via distorted Born iterative method. *Progress In Electromagnetics Research*, 2019, vol. 166, p. 23–41. DOI: 10.2528/PIER19072203

[22] ISERNIA, T., CROCCO, L., D'URSO, M. New tools and series for forward and inverse scattering problems in lossy media. *IEEE Geoscience and Remote Sensing Letters*, 2004, vol. 1, no. 4, p. 327–331. DOI: 10.1109/LGRS.2004.837008

[23] XU, K., ZHONG, Y., SONG, R., et al. Multiplicative-regularized FFT twofold subspace-based optimization method for inverse scattering problems. *IEEE Transactions on Geoscience and Remote Sensing*, 2015, vol. 53, no. 2, p. 841–850. DOI: 10.1109/TGRS.2014.2329032

About the Authors . . .

Amit MAGDUM (corresponding author) received his M.Tech. degree in Electronics Engineering from the Walchand College of Engineering Sangli, India in 2016. He is currently a Ph.D. student in the Department of Electronics and Communication Engineering at the National Institute of Technology Goa, India. His areas of interest include inverse problems, microwave imaging, and deep learning.

Mallikarjun ERRAMSHETTY received his M.Tech. and Ph.D. from the Indian Institute of Technology Kharagpur, India in 2009 and 2016, respectively. Presently, he is working as an Assistant Professor in the Department of Electronics and Communication Engineering at the National Institute of Technology Goa, India. His research interest includes microwave imaging, inverse problems, and terahertz imaging.

Ravi Prasad K. JAGANNATH received his M.Sc. from the Indian Institute of Technology Delhi, India in 2008. He received his Ph.D. from the Indian Institute of Science Bangalore, India in 2014. Presently, he is working as an Associate Professor in the Department of Applied Sciences at the National Institute of Technology Goa, India. His research interest includes inverse problems, biomedical imaging, and numerical optimization.